The Astrophysical Journal, 600:781–788, 2004 January 10

SPECTROPOLARIMETRY AND MODELING OF THE ECLIPSING T TAURI STAR KH 15D

Eric Agol,[1,2,3] Aaron J. Barth,[4,5] Sebastian Wolf,[4] and David Charbonneau[4]

Received 2003 July 25; accepted 2003 September 19

ABSTRACT

KH 15D is a strongly variable T Tauri star in the young star cluster NGC 2264 that shows a decrease in flux of 3.5 mag lasting for 18 days and repeating every 48 days. The eclipsing material is likely due to orbiting dust or rocky bodies in a partial ring or warped disk that periodically occults the star. We measured the polarized spectrum in and out of eclipse at the Keck and Palomar observatories. Outside of the eclipse, the star exhibited low polarization consistent with zero. During eclipse, the polarization increased dramatically to $\sim$2% across the optical spectrum, while the spectrum had the same continuum shape as outside of eclipse and exhibited emission lines of much larger equivalent width, as previously seen. From the data, we conclude that (1) the scattering region is uneclipsed, (2) the scattering is nearly achromatic, and (3) the star is likely completely eclipsed so that the flux during eclipse is entirely due to scattered light, a conclusion also argued for by the shape of the ingress and egress. We argue that the scattering is not due to electrons but may be due to large dust grains of size $\sim$10 μm, similar to the interplanetary grains that scatter the zodiacal light. We construct a warped-disk model with an extended dusty atmosphere that reproduces the main features of the light curve, namely, (1) a gradual decrease before ingress due to extinction in the atmosphere (similar for egress), (2) a sharper decrease within ingress due to the optically thick base of the atmosphere, and (3) a polarized flux during eclipse that is 0.1% of the total flux outside of eclipse, which requires no fine-tuning of the model. The inclination of the warp is set by the duration of ingress and egress assuming that the warp is located at the Keplerian radius, and the inclination of the observer is then determined by the duration of the eclipse.

Subject headings: eclipses — polarization — stars: individual (KH 15D) — stars: pre–main-sequence — stars: variables: other

On-line material: color figures, mpeg animation

1. INTRODUCTION

T Tauri stars are thought to be young stars that are still accreting gas through a disk. Kearns & Herbst (1998) discovered the T Tauri star KH 15D (K7 V, $d = 760$ pc), which shows an eclipse for $\frac{1}{3}$ of its period, implying that it is obscured by faint circumstellar material rather than a stellar companion; earlier data showed the star rebrighten at mid-eclipse, although this has weakened in recent data (Hamilton et al. 2001). This indicates that the obscuring material subtends a large angle, which may herald the presence a low-mass stellar companion to shepherd the material via resonant interaction or to create a distorted disk (Bryden et al. 2000). In addition, the duration of the eclipse trough is lengthening over time, changing from 16 days to 18 days over 5 years, and data from 50–90 years ago showed no evidence for eclipses (Winn et al. 2003), which means that the obscuring material is rapidly evolving. During eclipse, residual flux is still present at a level of $\sim$1/20 of the flux outside of eclipse indicating that (1) the obscuring material is porous (covering factor is less than 1), (2) the eclipse is total, but scattered light "fills in" the eclipse, creating some residual flux, or (3) some flux is scattered and some transmitted. The scattering interpretation may be favored as the star becomes slightly bluer during eclipse as one would expect from scattered light, although the fluctuations in color are comparable to the color difference (Herbst et al. 2002). In addition, the equivalent width of Hα increases dramatically from 2 to $\sim$30 Å, indicating a change from an unobscured "weak-line" T Tauri star to a classical T Tauri star!

The eclipse provides a natural "coronagraph" during which the suppression of stellar light allows any scattering by surrounding material to become more prominent. We attempted to distinguish the above possibilities by carrying out spectropolarimetry inside and outside of the eclipse. Since the unpolarized flux of the star dilutes the percentage of polarization, we expected that the percentage polarization due to scattered light would increase by a factor of at least 20 during the eclipse if the scattering material lies exterior to the occulting material and if the starlight is intrinsically unpolarized. This scenario is analogous to type 1 active galactic nuclei (AGNs), which are unobscured and show low polarization, versus type 2 AGNs, which are obscured and show much higher polarization (Antonucci 1993). Some T Tauri stars show an anticorrelation between total flux and polarization (e.g., Mekkaden 1999; Ménard et al. 2003), which may be exaggerated in KH 15D as the flux variations are much more extreme. On the other hand, if the residual flux is only due to incomplete coverage by the occulting material, then the polarization will not change. Interstellar foreground polarization, which is measured to be 0.1%–0.4% in the V band for NGC 2264 (Breger & Dyck 1972), will not change during eclipse. Before our observations, the optical polarization of

[1] Theoretical Astrophysics, MS 130-33, California Institute of Technology, Pasadena, CA 91125; agol@tapir.caltech.edu.
[2] *Chandra* Fellow.
[3] Department of Astronomy, University of Washington, Box 351580, Seattle, WA 98105; agol@astro.washington.edu.
[4] Department of Astronomy, MS 105-24, California Institute of Technology, Pasadena, CA 91125.
[5] *Hubble* Fellow.

KH 15D had not yet been measured, but during eclipse it shows the characteristics of classical T Tauri stars, which have a mean polarization of 1.2% with a standard deviation of 0.8% and maximum polarization of 2.5% (Ménard 1991).

In § 2 we summarize the spectropolarimetric observations, in § 3 we give the results of the observations, in § 4 we discuss the implications of these results for models of this T Tauri star, and in § 5 we review our conclusions.

2. OBSERVATIONS

The primary observational goal was to measure the difference in polarization between eclipse and noneclipse. Outside eclipse, the star is sufficiently bright to observe at the Palomar 200 inch telescope ($V \sim 16$), but during the eclipse the star is a factor of $\sim$20 fainter, which required using Keck to obtain a similar number of photons in a reasonable observing time. The Palomar observations were taken with the Double Spectrograph spectropolarimeter (Oke & Gunn 1982; Goodrich 1991), while the Keck I observations were taken with the Low Resolution Imaging Spectrograph polarimeter (Oke et al. 1995; Goodrich 1991). Both instruments add dual-beam polarimetry optics to a double spectrograph incorporating dichroics to separate the blue and red beams. The observations and reductions were done using standard spectropolarimetry techniques (Miller, Robinson, & Goodrich 1988). The observations of KH 15D were performed in sequences of four 15 minute exposures at four different positions of a rotating half-wave plate. Each four-exposure sequence allows measurement of the Stokes parameters q and u. For each hour of observations, the position angle of the spectrograph slit was aligned with the parallactic angle for the midpoint of the hour. The instrumental setup is described in Table 1, while the observational summary is given in Table 2. Null, polarized, and flux standards were observed during each night. Since instrumental polarization can be present in the Palomar 200 inch (Ogle et al. 1999), we observed four null standards each at two perpendicular slit position angles. We used the measured polarization of the null standards as an estimate of the mean and uncertainty of the instrumental polarization, and we subtracted the mean instrumental Stokes parameters q and u from the measured Stokes parameters of KH 15D to correct for the instrumental polarization. At Palomar the instrumental polarization was found to be $0.30\% \pm 0.22\%$ over 4600–5600 Å and $0.13\% \pm 0.13\%$ over 5650–8500 Å. At Keck the instrumental polarization was negligible, less than 0.1%. At Palomar the observations were obtained through clouds, while the Keck nights were mostly clear, but not photometric.

A 7th magnitude B2 III star, HD 47887, is located 39″ away from KH 15D. In the Keck observations a diffraction spike from this bright star periodically swept through the slit, passing within several arcseconds of KH 15D in several exposures. In these exposures sky subtraction was difficult, making it impossible to accurately measure the polarization and also adversely affecting the color of the extracted spectra for 2 of the 6 hours.

Figure 1 depicts the phase of our observations with respect to the 48.36 day period of KH 15D.

TABLE 1
INSTRUMENTAL SETUP

Instrument, Side	Wavelength Range (Å)	Resolution (Å pixel^{-1})
DBSP, red.....	5620–8120	2.45
DBSP, blue.....	3350–5750	3.38
LRISp, red.....	3200–5850	2.0
LRISp, blue.....	5650–9400	2.0

NOTE.—DBSP: Double Spectrograph spectropolarimeter; LRISp: Low Resolution Imaging Spectrograph polarimeter.

3. RESULTS

The continuum polarization in the Keck and Palomar data was measured over wavelength bins of width 1000 Å. We averaged the three measurements from Palomar and subtracted off the mean polarization measured from observations of four null-standard stars. We computed the mean of four measurements from Keck, and the error bars were computed from the standard deviation of these measurements plus the statistical error of the individual measurements. The Palomar data show a small enough polarization and large enough errors that the data are consistent with being unpolarized at the $\sim 1\ \sigma$ level (see Fig. 2). However, the Keck data showed a much higher polarization and are inconsistent with the Palomar data at a high significance. Tables 3 and 4 summarize the polarization measurements of the eclipsed and uneclipsed data. The eclipsed data show a slight increase in polarization from the blue (4600–5600 Å) to the red (7000–8000 Å) at 3 σ significance. Most of this change is due to an increase in the q Stokes parameter (Fig. 2), while u remains constant; however, the errors are large enough that a change in the polarization angle is only significant at 1.5 σ.

Figure 3 shows the total flux spectrum in and out of eclipse. The spectral shape appears nearly identical in and out of eclipse, despite the change in total flux of $\sim$3.5 mag. We measured the mean of the ratio of the uneclipsed to the eclipsed data in each of the three bands (4600–5600, 6000–7000, and 7000–8000 Å), excluding the emission lines, and computed the standard deviation of the ratio within each band, which is reported in Table 3. The flux ratios differ between the bluest (4600–5600 Å) and reddest (7000–8000 Å) bands by only 1 σ, which is statistically consistent with no color change. The absolute value of the uneclipsed to eclipsed flux ratios are not to be trusted as the nights were not photometric, so we report only the ratio of each band to the 6000–7000 Å band. For comparison with the photometric data of Herbst et al. (2002) we also computed synthetic photometry of our spectra which gave $V-R = 0.81$ mag and $V-I = 1.45$ mag during eclipse and $V-R = 0.79$ mag outside of eclipse, which are in agreement with the range of values reported by Herbst et al. (2002). We estimate the uncertainty on these colors to be $\sim$0.1 mag as there appear to be differences between individual spectra on scales of $\sim$500 Å that may be due to fluctuations in the flat fields, difficulty of sky subtraction, overall systematic uncertainties in flux calibration, or other instrumental variations.

There are a large number of stellar photospheric features which are seen in both spectra and are indicative of a K6 V spectral type with $T_{\rm eff} \sim 4300$ K, somewhat hotter than the K7 V type estimated by Hamilton et al. (2001), which may be due to the fact that our spectrum covers bluer wavelengths. Almost all of these features show the same equivalent widths in both spectra, indicating that the eclipsed spectrum is a scaled version of the uneclipsed spectrum. We have measured the Lick indices (Worthey & Ottaviani 1997) for both the eclipsed and uneclipsed spectra, plotted in Figure 4. The Hδ indices are

TABLE 2
OBSERVATIONAL SUMMARY

Date (UT)	Telescope	Exposure Time (hr)	Slit Width (arcsec)	Conditions
2003 Jan 25.....	Palomar	3	2.0	Partly cloudy
2003 Feb 23.....	Keck	3	1.5	Partly cloudy
2003 Feb 24.....	Keck	1	1.0	Clear
2003 Feb 25.....	Keck	2	1.5	Clear

contaminated by the [S II] emission line in the Keck data. The Na D equivalent width is smaller during the eclipse, which we attribute to unobscured Na D emission filling in the absorption line. The measured indices for KH 15D agree best with those of a K6 V star; the agreement is good enough that there is no evidence for optical veiling. The Hα emission line has a much higher flux in the eclipsed spectrum than in the uneclipsed spectrum by a factor of $\sim$3.3 (since our data were not photometric, this factor is probably $\sim$2.7). This may be partly due to variability and partly due to partial eclipse of the Hα line as Hamilton et al. (2003) found that the flux of Hα could decrease or increase during eclipse and the shape of Hα varied significantly as well. They measured an equivalent width of 2 Å outside eclipse and 40–70 Å in eclipse, compared with our measurements of 3 and 30 Å, respectively. In addition, four emission lines appear in the eclipsed spectrum that are not apparent in the uneclipsed spectrum. The fluxes and equivalent widths of the emission lines are given in Table 5, which we have computed by subtracting off a continuum template, with errors estimated from the standard deviation of the residuals. Included is the Na D absorption line at 5890 Å, which is stronger in the uneclipsed spectrum than in the eclipsed spectrum (we have used the uneclipsed spectrum as the continuum template for this line).

4. DISCUSSION

The variation of the polarization between eclipse and noneclipse indicates that the *scattering region is not completely obscured by the occulting material*. If the occulter completely blocks all the light from the star, if the scattering is nearly isotropic, and if the scattering region is nearly spherically symmetric, then the residual flux, $\sim$5%, indicates that the optical depth of the unobscured scattering material is $\sim$0.05. Since the spectra inside and outside eclipse are consistent with no change in the spectral shape, and since the spectrum within eclipse is consistent with very weak wavelength dependence of the polarization, we conclude that the scattering mechanism is nearly achromatic, implying that the scatterers may be electrons or large grains. We discuss each of these possibilities in turn.

4.1. *Electron Scattering*

If the scattering mechanism were electrons, then the low measured polarization of 2% indicates that the scattering region need be only slightly asymmetric. For example, in the model of Brown & McLean (1977), the polarization caused by an axisymmetric Thomson scattering envelope is $P = \sin^2 i/(2\alpha + \sin^2 i)$, where α is a "shape factor" that depends on the precise geometry of the scatterers. Since the eclipsing region is likely in the equatorial plane of the circumstellar material, we can assume that $i \sim 90^\circ$. Thus, $\alpha \sim 25$ for $P \sim 2\%$. For a scattering geometry which consists of a slightly oblate or prolate spheroid of axis ratio $a = 1 + \epsilon$, then $\alpha \sim 5/\epsilon$, so $|\epsilon| \sim 0.2$ to create the observed polarization; i.e., only a 20% deviation from spherical symmetry is required to give the measured polarization. Note that this example is simply illustrative since we have no preferred model for the scattering region.

If we assume that all of the light during eclipse is due to electron scattering, then we can estimate the bound-free continuum emission expected from this gas. Consider a nearly symmetric region of uniform electron density and temperature surrounding the star of size r_{es}. We assume that the eclipsing material is located near the Keplerian radius, r_{Kep}, for a 48 day

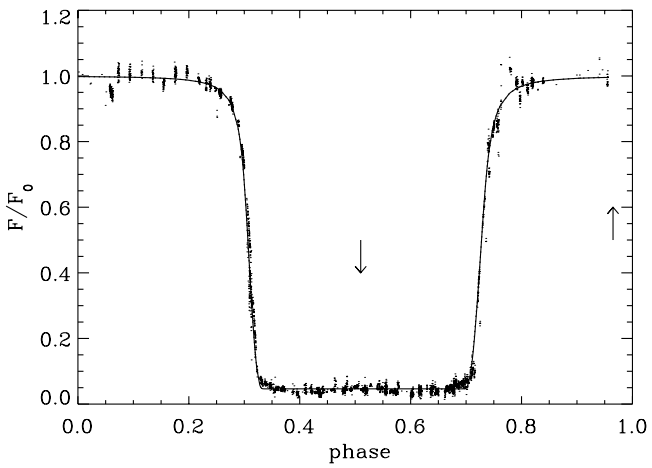

FIG. 1.—Phased light curve of KH 15D from the 2001–2002 campaign (Herbst et al. 2003). The arrows indicate the phases of our observations. The solid line is a model fit to the data described in § 4.3.

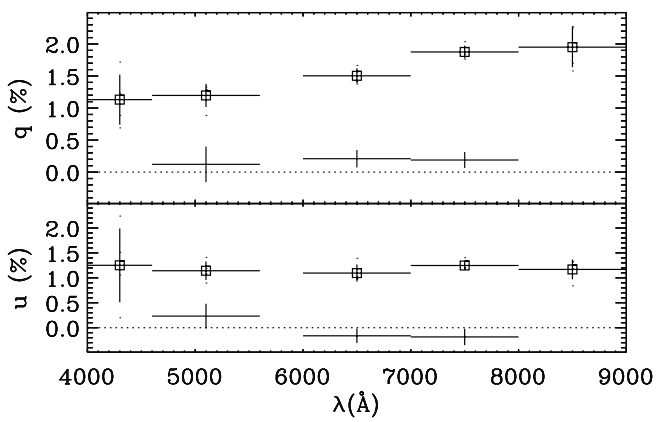

FIG. 2.—Normalized Stokes parameters q and u of KH 15D. The squares are the data in eclipse, while the plus signs are data out of eclipse. Horizontal bars represent the wavelength ranges over which the Stokes parameters were measured.

TABLE 3
PALOMAR OBSERVATIONAL SUMMARY

Band (Å)	p (%)	θ_p (deg)	$\langle F_{un}/F_{ec}\rangle$[a]
4600–5600.....	0.26 ± 0.25	31 ± 27	1.00 ± 0.04
6000–7000.....	0.17 ± 0.21	−19 ± 35	1
7000–8000.....	0.16 ± 0.23	−22 ± 41	1.05 ± 0.04

[a] The mean of the ratio of the uneclipsed (Palomar) flux to the eclipsed (Keck) flux within the given band, emission lines excluded, divided by the ratio in the 6000–7000 Å band.

period. The low polarization implies that the electron scattering region must be at a larger radius, $r_{es} > r_{Kep} \sim 0.2$ AU, to avoid becoming too asymmetric due to obscuration. Since the material is nearly symmetric, the mean optical depth of the scattering region is $\tau_{es} \sim 0.05$, which implies an electron number density of $n_e < 2 \times 10^{10}$ cm^{-3} (assuming a uniform density). The bound-free emission expected at, say, 6000 Å must be less than $F_\nu \sim 10^{-28}$ ergs cm^{-2} s^{-1} Hz^{-1} to avoid changing the strength of the Lick indices. Computing the emission from an optically thin spherical region of plasma in LTE, we find that $T > 2 \times 10^6$ K to be consistent with this upper limit. Note that this is a strong lower limit since it is likely that the scattering region need be larger to give the small observed polarization. In addition, one can place a constraint on the temperature based on the strength of Balmer line emission; however, the interpretation is complicated by the unknown optical depth of the Balmer lines. Even so, the lower limit on the temperature based on the lack of detected bound-free emission is 4 times the virial temperature at r_{Kep}, meaning that this gas would be strongly unbound and will outflow in less than a dynamical timescale, implying a mass-loss rate of 10^{-7} $M_\odot$ yr^{-1}, which is rather large for a weak-line T Tauri star. Thus, it is more likely that the scattering is not due to electrons but may be due to large dust grains, which we discuss next.

4.2. *Dust Scattering*

If the scattering were due to dust, then the grain sizes would have to be fairly large to allow the weak wavelength dependence of the polarization *and* flux. This is true for the zodiacal light, which reflects an optical spectrum that is identical to that of the Sun (Leinert et al. 1998). On the basis of the achromaticity of the zodiacal scattering, the scatterers are thought to be large dust grains, 10–100 μm in size, and there is further evidence that these grains might be quite "fluffy" (i.e., low filling factor) with densities as low as $\rho_f \sim 0.25$ g cm^{-3}.

For the estimation of the wavelength dependence of the scattering and polarization by dust particles we approximate the particles as spheres (Mie scattering) and compute the polarized differential scattering cross section by single particles using a standard approach (Voshchinnikov 2002; Wiscombe 1980; Bohren & Huffman 1983; Wolf 2003).[6] We have chosen the distribution of refractive indices of the materials from Weingartner & Draine (2001): 62.5% astronomical silicate and 37.5% graphite. Since graphite is crystalline, it was considered as two "different" materials in the computation: the first with a refractive index as measured perpendicular to the crystal rotation axis, 25%, and the second parallel, 12.5%. We assumed that distribution of the dust size, a, follows a power law $dn/da \propto a^{-\alpha}$ for $a_{min} < a < a_{max}$, and derived the scattering properties of the ensemble of particle species and sizes (Martin 1978; S. Wolf & N. V. Voshchinnikov, in preparation).

We averaged the scattered polarized flux over the entire 4π steradians divided by the total scattered flux to estimate the mean polarization as a function of wavelength for each dust model. We then compared this to the relative wavelength dependence of the measured polarization (the absolute polarization depends on the exact geometry of the scattering region, which is unknown; see the next section for one particular model). We also compared the relative wavelength dependence of the scattered flux by dividing the eclipsed spectrum by the uneclipsed spectrum. Given the assumptions that (1) the wavelength dependence of the flux and polarization does not depend on the geometry of the scatterers and (2) the scatterers can be described by a single power law, we can then place a constraint on the parameters of the dust model. We find that the lower limit, a_{min}, does not change the fit much, so we

[6] The code for calculation of the Mie scattering coefficients is available at http://mc.caltech.edu/~swolf/miex-web/miex.htm—or contact the authors.

TABLE 4
KECK OBSERVATIONAL SUMMARY

Band (Å)	p (%)	θ_p (deg)
4000–4600.....	1.46 ± 0.70	23.9 ± 14
4600–5600.....	1.63 ± 0.19	21.8 ± 3.3
6000–7000.....	1.85 ± 0.14	18.0 ± 2.2
7000–8000.....	2.25 ± 0.10	16.8 ± 1.2
8000–9000.....	2.24 ± 0.29	15.5 ± 3.7

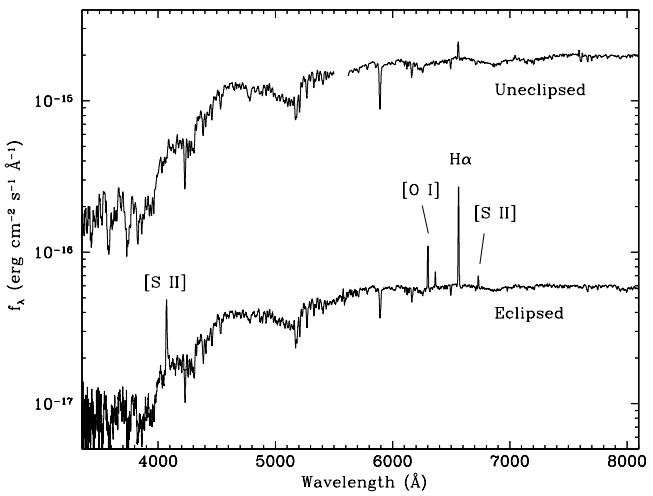

FIG. 3.—Spectrum out of eclipse (*top line*) and in eclipse (*bottom line*)

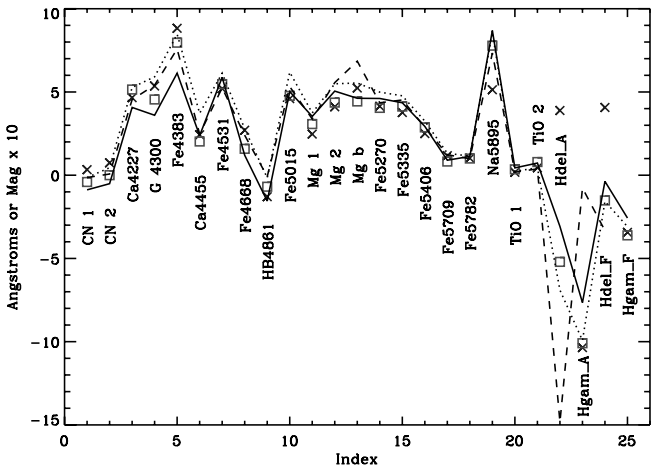

FIG. 4.—Lick spectral indices for the eclipsed (*crosses*) and uneclipsed (*squares*) data, as well as a K7 V star (*solid line*), K6 V star (*dotted line*), and K5 V star (*dashed line*). Note that the molecular band indices with units of magnitudes (CN, Mg, and TiO) have been multiplied by a factor of 10 for clarity. The index numbers are taken from Worthey & Ottaviani (1997). [*See the electronic edition of the Journal for a color version of this figure.*]

simply vary $1\ \mu\mathrm{m} < a_{\max} < 100\ \mu\mathrm{m}$ and $0 < \alpha < 2$. The minimum χ^2 is 12 for five data points for $a_{\max} = 8\ \mu$m and $\alpha = 0$, with the confidence contours plotted in Figure 5. At 90% confidence, $\alpha < 2$ and $5\ \mu\mathrm{m} < a_{\max} < 10\ \mu$m, which indicates that the scattering is dominated by large dust grains. Unfortunately, the minimum reduced $\chi_r^2 = 2.2$, which is rather large. This is due to the fact that the measured polarization increases toward longer wavelengths, while the dust scattering models predict a polarization that is nearly constant, or slightly decreasing, with wavelength.

The opacity of large dust grains scales as $\kappa/\rho = 0.75a^{-1}\ \rho^{-1} \sim 3 \times 10^3 a_{10}^{-1}(\rho_f/\rho)$ cm^2 g^{-1}, where $a_{10} = a/10\ \mu$m. Thus, the Eddington limit for the smaller of the large dust grains scales as $L_{\mathrm{Edd,dust}} = 1.7 \times 10^{34} a_{10}(\rho/\rho_f)$ ergs s^{-1}, which is similar to the luminosity of KH 15D, $L_{\mathrm{KH15D}} \sim 2.4 \times 10^{33}$ ergs s^{-1}. Thus, smaller dust grains will be removed from the system by radiation forces. In addition, radiation forces on the larger grains may be significant enough to modify the structure of the system.

4.3. *Scattering Model*

Herbst et al. (2002) have proposed a model for the occulter that consists of a semi-infinite edge crossing the star. This model is attractive as the finite size of the star and limb darkening can account for the shape of the ingress and egress, and, if the occulter is at the Keplerian radius, then it must be inclined to the orbital plane by 15° to give the correct duration of ingress and egress. However, we have found that the ingress and egress of the eclipse (Fig. 1, near phase of 0.3 and 0.7) show a more gradual rolloff than expected for a semi-infinite occulter. This can be fitted with an optical depth of the occulter that scales with position as $\tau \propto x^{-2}$, where x is the coordinate perpendicular to the edge of the occulter, which gives an excellent fit to the phased light-curve data (solid line in Fig. 1).

This material causing extinction will scatter as well, and in the case of large grains there will be significant forward scattering (van de Hulst 1981). In fact, this may account for the scattered flux present during the eclipse; however, to compute the scattered light requires a knowledge of the three-dimensional distribution of scattering and occulting material, as well as a knowledge of the scattering properties. We construct such a model by assuming that (1) the occulter is located at the Keplerian radius and (2) the 15° tilt of the occulter is due to a warped disk. We model the material as a succession of tilted circular annuli, creating a warped disk, with the tilt angle given by

$$i_{\mathrm{tilt}} = i_w \exp\left[-\frac{(r - r_w)^2}{2\sigma_w^2}\right], \qquad (1)$$

where r_w is the radius of maximum tilt, i_w is the maximum tilt, r is the radius in the disk, and σ_w is the width of the tilted region, and we assume that the nodes of the warped annuli are aligned. The observer we place at an angle i_{obs} to the equatorial plane, and we rotate the warped disk as a solid body with a period equal to that of KH 15D. In addition, we cut the disk off at $r_{\mathrm{in}} = 0.5r_w$ and $r_{\mathrm{out}} = 4r_w$. The opacity of the scattering material we distribute as $\kappa = \kappa_0[h(r/r_w)/(\theta - \pi + i_{\mathrm{tilt}})]^2$, to produce the observed rolloff in intensity, where h is the angular scale height, θ is the polar angle, and κ_0 is a fiducial opacity. We find a good fit to the light curve for $i_w = 17.^\circ 6$, $i_{\mathrm{obs}} = 6.^\circ 7$, $h = 1.^\circ 6$, $r_w = 0.22$ AU (this is the Keplerian radius), and $\sigma_w = r_w$. When taking into account only extinction, this distribution produces the solid light curve in Figure 1 after the addition of 4.5% of the uneclipsed flux during eclipse. However, part of the extinction is due to scattering, so we also have computed the singly scattered component of this density distribution assuming an albedo of unity and using the scattering function for zodiacal light derived by Hong (1985), which is strongly forward scattering and has a

TABLE 5
EMISSION LINES

Line (Å)	Flux[a] (10^{-15} ergs cm^{-2} s^{-1})	EW (Å)
Hα λ6563[b]	5.88 ± 0.71	3.2 ± 0.39
Hα λ6563	1.74 ± 0.19	29.7 ± 3.2
[S II] λ4069	0.362 ± 0.025	22.2 ± 1.5
Na D λ5890	0.153 ± 0.015	3.6 ± 0.36
[S II] $\lambda\lambda$6716, 6731	0.093 ± 0.013	1.6 ± 0.23
[O I] λ6300	0.397 ± 0.065	7.0 ± 1.1
[O I] λ6364	0.132 ± 0.017	2.3 ± 0.3

[a] The absolute value of these measured fluxes is unreliable due to nonphotometric conditions and slit losses.
[b] Uneclipsed line (the rest are eclipsed).

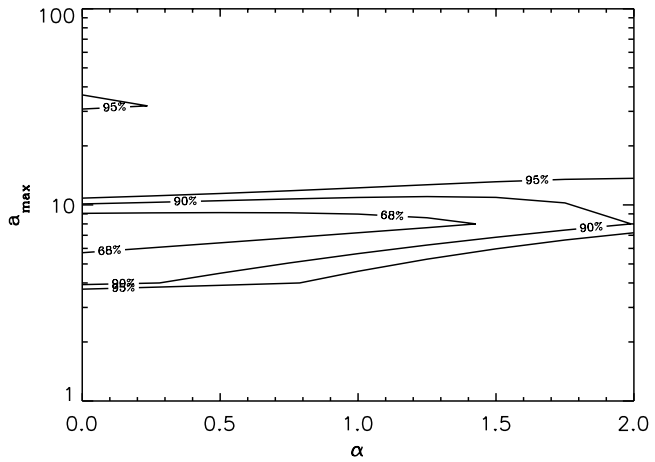

FIG. 5.—Confidence limits for dust models as a function of $a_{\max}$ and α

maximum polarization of 22%. We find that the polarized flux of the scattered light during eclipse is 0.1% of the unobscured total flux, which is the same as the observed polarized flux during eclipse of KH 15D (Fig. 6). Figure 7 shows the appearance of the scattered light in this model at mid-eclipse (an animated version of this figure that shows the appearance as a function of phase is available on-line).

One prediction of this model is that the polarization angle should vary by $\sim 15^\circ$ during the eclipse. However, the total model flux during mid-eclipse is only 2.5% of the uneclipsed flux, which is about half the observed mid-eclipse flux, indicating that there may be another component of scattered light that has low polarization, such as diffracted light, which is not taken into account in the model of Hong (1985), or backscattered light. In a future study we may carry out more sophisticated modeling, varying the radius of the warp as well as the symmetry of the warp, and including multiple scattering and varying the dust grain model, to see how the scattered flux varies with dust composition and with wavelength of the observed light, and we will see whether diffraction, multiple scattering, or backscattering can explain the brightening at mid-eclipse. There is evidence that the ingress and egress differ slightly in time between the even and odd eclipses, which may imply that the warp is an $m = 2$ mode rather than $m = 1$ as in our model. If so, the back warp will be partly eclipsed by the front warp, while the edges will be visible during mid-eclipse, which may explain the rebrightening. Alternatively, the symmetry during mid-eclipse of the front warp may cause a brightening due to diffraction, which is likely to be wavelength dependent. If the albedo is less than unity, then mid-infrared observations may point toward an $m = 2$ configuration if they also show a peak at mid-eclipse since the infrared light is emitted isotropically, similar to the backscattered light.

5. CONCLUSIONS

A summary of the results: (1) Near mid-eclipse the polarization is $\sim 2\%$, and is consistent with zero outside of eclipse ($0.2\% \pm 0.2\%$). Combined with other photometric data, the polarized flux near mid-eclipse is $\sim 0.1\%$ of the flux outside of eclipse. This indicates that there is an unobscured scattering region surrounding the T Tauri star that creates the polarization; the polarization cannot be solely due to foreground transmission effects (not associated with the star) as there would no variation. (2) The data are nearly consistent with no wavelength dependence of the polarization during eclipse. This indicates that the scatterers are approximately gray. In addition, electron scattering is unlikely to cause the observed polarization. (3) The spectrum within the eclipse is consistent with being a scaled version of the spectrum outside of eclipse with no wavelength dependence of the ratio except for the presence of stronger emission lines, which also argues for gray scattering; Rayleigh scattering is ruled out. Our Mie dust scattering model implies $\alpha < 2$ and $5\ \mu\text{m} < a_{\max} < 10\ \mu\text{m}$ at 90% confidence; however, the best-fit model is not an adequate fit. (4) The qualitative features of the eclipse can be reproduced by a model of a warped disk that orbits in front of the star, periodically eclipsing the star, having an extended atmosphere that causes a decrease in light before and after eclipse as well as scattered light within eclipse, which is consistent with the observed polarized flux. The polarization adds an extra clue that the eclipsing material completely occults the star since the maximum observed polarization of classical T Tauri stars is $\sim 2.5\%$ (Ménard 1991) and the KH 15D spectrum looks like that of a classical T Tauri star

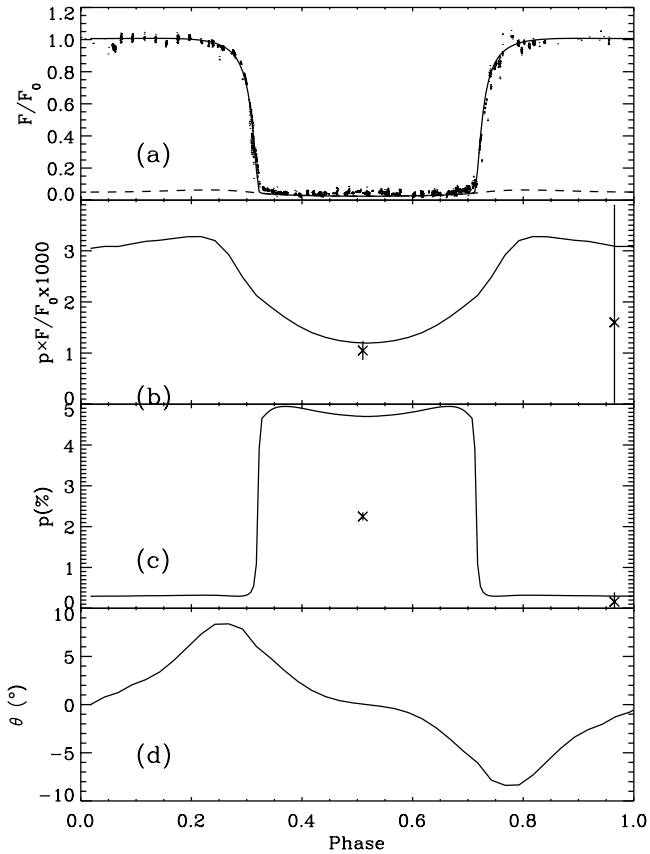

FIG. 6.—(*a*) Flux of KH 15D as a function of phase from Herbst et al. (2003), along with our model (*solid curve*) and the singly scattered light (*dashed curve*). (*b*) Model polarized flux normalized by F_0 at 7000–8000 Å (unity would be 100% polarized light). At mid-eclipse, we have taken our observed polarization and multiplied by the mean flux of the *I*-band observations near mid-eclipse by Herbst et al. (2003), $F/F_0 = 0.047 \pm 0.01$, since our observations were not photometric. The crosses with error bars show our observations, which agree remarkably well with the model. (*c*) Model polarization. Note the disagreement at mid-eclipse that may be due to an unpolarized component that also produces the disagreement in the total flux at mid-eclipse. (*d*) Polarization angle. We have not plotted the observed angles since we do not know the plane of the disk on the sky and our temporal coverage is not sufficient to determine the shape of $\theta(t)$.

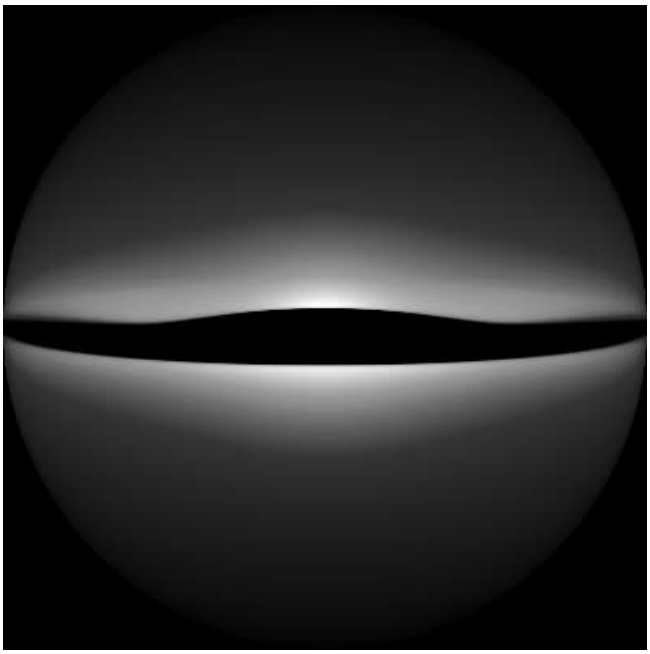

FIG. 7.—Scattered light at mid-eclipse for the model described in the text. [*See the electronic edition of the Journal for a color version of this figure and an mpeg animation.*]

during eclipse. This adds to the evidence that the eclipse is complete on the basis of (*a*) the steep egress and ingress, (*b*) the flat bottom of the trough of the eclipse, and (*c*) the fine-tuning that would be required to arrange 95% covering. It is interesting that the trough of the eclipse does show some slight variations, namely, an increase near mid-eclipse, which may indicate that the scattering region is partially eclipsed and this eclipse varies with time. It would be interesting to measure the polarization as a function of time within the eclipse to look for variation.

We have modeled the eclipse with a warped disk since a discrete cloud would be sheared in 10 orbits, while the eclipses have repeated with similar durations for $\sim$50 orbits. However, this does not mean that the warped disk model is without its own problems: If the warped model is correct, what drives the warp at such a short period? The interaction of the stellar magnetosphere is proposed to cause a similar occulting behavior in the T Tauri star AA Tauri (Bouvier et al. 1999); however, this star has a much short period between occultations, 8 days, while the longer period of KH 15D is much longer than the spin period of any known T Tauri star. One can place a lower limit on the warp radius of $r_{\rm min} = 10R_*$ since inward of this radius the warp would have to be at greater than 45° to create the correct duration of ingress due to the finite size of the star. At $r_{\rm min}$, the Keplerian period is 0.8 days, while a warp precession timescale is typically much longer than the Keplerian timescale. It may be that a planet excites a wave in the disk (Winn et al. 2003) or that an elongated dusty vortex causes obscuration (Barge & Viton 2003); each of these models might be consistent with the observed polarization profile, which remains to be quantified with a scattering calculation similar to the one presented here.

Future observations of interest would be to (1) measure the magnitude and angle of polarization throughout ingress and/or egress to test the warp model, (2) measure the polarization at higher spectral resolution within the Hα emission line to see whether it is unpolarized, and (3) look for variations of the flux during eclipse to determine whether the stellar variability is washed out by the time delays from scattering (although this requires a rather extended scattering region). In addition, near- and mid-infrared observations may show fluctuations if the occulting region has a warped geometry, as we have suggested.

We thank Catrina Hamilton, Lynne Hillenbrand, Patrick Ogle, and Russel White for useful discussions and Marshall Cohen for exchange of observing time. We thank Bill Herbst for providing published photometric data. Some of the data presented herein were obtained at the W. M. Keck Observatory, which is operated as a scientific partnership among the California Institute of Technology, the University of California, and the National Aeronautics and Space Administration. The Observatory was made possible by the generous financial support of the W. M. Keck Foundation. The authors wish to recognize and acknowledge the very significant cultural role and reverence that the summit of Mauna Kea has always had within the indigenous Hawaiian community. We are most fortunate to have the opportunity to conduct observations from this mountain.

Support for E. A. was provided by the National Aeronautics and Space Administration through *Chandra* Postdoctoral Fellowship Award PF0-10013 issued by the *Chandra X-ray Observatory* Center, which is operated by the Smithsonian Astrophysical Observatory for and on behalf of the National Aeronautics Space Administration under contract NAS 8-39073. S. Wolf was supported by NASA through grant NAG 5-11465.

Research by A. J. B. is supported by NASA through *Hubble* Fellowship grant HST-HF-01134.01-A awarded by STScI, which is operated by AURA, Inc., for NASA, under contract NAS 5-26555.

REFERENCES

Antonucci, R. 1993, ARA&A, 31, 473
Barge, P., & Viton, M. 2003, ApJ, 593, L117
Bohren, C. F., & Huffman, D. R. 1983, Absorption and Scattering of Light by Small Particles (New York: John Wiley & Sons)
Bouvier, J., et al. 1999, A&A, 349, 619
Breger, M., & Dyck, H. M. 1972, ApJ, 175, 127
Brown, J. C., & McLean, I. S. 1977, A&A, 57, 141
Bryden, G., Różyczka, M., Lin, D. N. C., & Bodenheimer, P. 2000, ApJ, 540, 1091
Goodrich, R. 1991, PASP, 103, 1314
Hamilton, C. M., Herbst, W., Mundt, R., Bailer-Jones, C. A. L., & Johns-Krull, C. M. 2003, preprint (astro-ph/0305477)
Hamilton, C. M., Herbst, W., Shih, C., & Ferro, A. J. 2001, ApJ, 554, L201
Herbst, W., et al. 2002, PASP, 114, 1167
Hong, S. S. 1985, A&A, 146, 67
Kearns, K. E., & Herbst, W. 1998, AJ, 116, 261
Leinert, Ch., et al. 1998, A&AS, 127, 1
Martin, P. G. 1978, Cosmic Dust: Its Impact on Astronomy (Oxford: Clarendon)
Mekkaden, M. V. 1999, A&A, 344, 111
Ménard, F. 1991, in IAU Colloq. 129, Structure and Emission Properties of Emission Disks, ed. C. Bertout S. Collin-Souffrin, & J. P. Lasota (Gif-sur-Yvette: Editions Frontières), 59
Ménard, F., Bouvier, J., Dougados, C., Melnikov, S. Y., & Konstantin, N. G. 2003, A&A, 409, 163
Miller, J. S., Robinson, L. B., & Goodrich, R. W. 1988, in Instrumentation for Ground-Based Optical Astronomy, ed. L. B. Robinson (New York: Springer), 157

Ogle, P. M., Cohen, M. H., Miller, J. S., Tran, H. D., Goodrich, R. W., & Martel, A. R. 1999, ApJS, 125, 1
Oke, J. B., & Gunn, J. E. 1982, PASP, 94, 586
Oke, J. B., et al. 1995, PASP, 107, 375
van de Hulst, H. C. 1981, Light Scattering by Small Particles (New York: Dover)
Voshchinnikov, N. V. 2002, Astrophys. Space Phys. Rev., 12, 1
Weingartner, J. C., & Draine, B. T. 2001, ApJ, 548, 296
Winn, J. N., Garnavich, P. M., Stanek, K. Z., & Sasselov, D. D. 2003, ApJ, 593, L121
Wiscombe, W. J. 1980, Appl. Opt., 19, 1505
Wolf, S. 2003, Comput. Phys. Commun., 150, 99
Worthey, G., & Ottaviani, D. L. 1997, ApJS, 111, 377